Influence of the aerodynamic drag on the motion of interplanetary ejecta

Bojan Vršnak
Hvar Observatory, Faculty of Geodesy, Zagreb, Croatia

Nat Gopalswamy
Department of Physics, Catholic University of America, Washington, D. C., USA

Received 29 April 2001; revised 14 August 2001; accepted 12 September 2001; published XX Month 2002.

[1] A simple semi-empirical model for the motion of interplanetary ejecta is proposed to advance the prediction of their arrival times at Earth. It is considered that the driving force and the gravity are much smaller than the aerodynamic drag force. The interaction with the ambient solar wind is modeled using a simple expression for the acceleration $\dot{\upsilon} = -\gamma(\upsilon - w)$, where $w = w(R)$ is the distance-dependent solar wind speed. It is assumed that the coefficient γ decreases with the heliocentric distance as $\gamma = \alpha R^{-\beta}$, where α and β are constants. The equation of motion is integrated numerically to relate the Earth transit time and the associated in situ velocity with the velocity of coronal mass ejection. The results reproduce well the observations in the whole velocity range of interest. The model values are compared with some other models in which the interplanetary acceleration is not velocity dependent, as well as with the model where the drag acceleration is quadratic in velocity $\dot{\upsilon} = -\gamma_2(\upsilon - w)|\upsilon - w|$. *INDEX TERMS:* 2164 Interplanetary Physics: Solar wind plasma, 2111 Interplanetary Physics: Ejecta, driver gases, and magnetic clouds, 7513 Solar Physics, Astrophysics, and Astronomy: Coronal mass ejections, 7531 Solar Physics, Astrophysics, and Astronomy: Prominence eruptions

1. Introduction

[2] Coronal mass ejections (CMEs) are propelled through the solar corona and launched into the solar wind by the Lorentz force [see, e.g., *Chen*, 1989, 1996; *Vršnak*, 1990, 1992, and references therein]. Acceleration maximum is usually observed within a distance of several solar radii [*Vršnak*, 2001a]. It has been shown by *Vršnak* [2001a] that the most abrupt eruptions are related to the so-called flare sprays which attain the maximum acceleration at low heights below 1 solar radius ($r_\odot$). In extreme cases the plane of sky acceleration is larger than 2000 m s^{-2}, and the velocity grows at the rate $\omega = \Delta\upsilon/\Delta h > 10^{-2}$ s^{-1} (υ is the velocity and h is the height). On the other hand, CMEs that achieve acceleration maximum at several $r_\odot$ show acceleration of the order of 10–100 m s^{-2} and the velocity growth rate of the order of 10^{-4} s^{-1}. After the acceleration phase most of CMEs show in coronographic observations an approximately constant velocity [*St. Cyr et al.*, 1999].

[3] In the interplanetary (IP) space, fast ejecta decelerate, whereas the events that are slower than the solar wind experience a prolonged acceleration: Statistically, CMEs show a larger span of speeds than IP ejecta at Earth (1 AU), the velocities converge toward the solar wind speed [see *Gopalswamy et al.*, 2000, and references therein]. Indirectly, the effect is also reflected in the difference between transit and in situ velocities of the shocks driven by the IP ejecta [see, e.g., *Watari and Detman*, 1998, and references therein].

[4] In fact, the coronographic observations reveal that in a significant fraction of fast CMEs the deceleration begins already in the high corona. *St. Cyr et al.* [1999] found that about 10% out of 76 events simultaneously observed by Mauna Loa coronameter and Solar Maximum Mission coronograph showed a negative acceleration. *Vršnak* [2001a] reported a deceleration in 14 out of 44 events (32%) in which the post-acceleration phase was observed. Twelve of these events were studied in detail by *Vršnak* [2001b] (hereinafter called paper 1). Inspecting the data shown in paper 1 one finds that the observed coronal decelerations of fast CMEs are at least an order of magnitude higher than the average IP decelerations found by *Gopalswamy et al.* [2000] for the events of similar initial velocities. This indicates that the main deceleration of fast ejecta takes place in the high corona after the driving force becomes negligible. On the other hand, a more efficient "early" acceleration of slow CMEs to the solar wind speed can partly explain shorter 1-AU transit times of such events than predicted by the constant acceleration model used by *Gopalswamy et al.* [2000]. Assuming a stronger acceleration in the early phase of the IP motion provides a higher average velocity of slow events and thus a shorter model travel time. However, let us note that the transit times of about 3 days found for some CMEs with observed coronal velocities between 200 and 400 km s^{-1} can be fully explained only by underestimated initial speeds due to projection effects (N. Gopalswamy et al., Validation and testing of empirical CME arrival model, submitted to *Journal of Geophysical Research*, 2001)(hereinafter referred to as Gopalswamy et al., submitted manuscript, 2001).

[5] In paper 1 it was demonstrated that the deceleration of the 12 studied events is velocity dependent and can be interpreted as a consequence the drag force (ad hoc attributed therein to the viscosity). This indicates that the interaction between the moving magnetic flux rope and the ambient solar wind plays a key role in the IP motion of CMEs, since at large distances it is expected that the Lorentz force driving the eruption, as well as the gravity, become negligible [*Chen*, 1996].

[6] The moving magnetic flux rope and the ambient magnetoplasma interact in a complex manner. There are several effects that should be taken into account. The magnetic flux rope expands; that is, its cross section increases. The speed, plasma density, and the

0148-0227/02/2001JA000120$09.00

magnetic field of the solar wind change with the distance. The three-dimensional aspect of the problem is essential, making the modeling difficult. Furthermore, the magnetic rope is not a rigid body, and its shape changes because of the coupling. Finally, the dissipative phenomena associated with the electric resistivity (providing the reconnection of the magnetic field of the rope with the solar wind field) and the viscosity could be also important.

[7] The subject was approached in different ways to model various aspects of the problem [see, e.g., *Wu et al.*, 1981; *Dryer et al.*, 1984; *Osherovich et al.*, 1993; *Vandas et al.*, 1995, 1996; *Cargill et al.*, 1995, 1996; *Gosling and Riley*, 1996]. Let us emphasize here the numerical simulations by *Cargill et al.* [1995, 1996], where the aerodynamic coupling was investigated and interpreted in detail. The flux rope was driven through the ambient magnetoplasma applying an ad hoc acceleration. Neglecting the viscosity, it was shown that the effect of the aerodynamic drag in the case when the external magnetic field is aligned with the rope's axis can be expressed well by the acceleration in the form $a = -c_D\rho_e\lambda|V|V/m$, where ρ_e is the external density, V is the velocity of the rope, λ is its radius, and $m = \pi\lambda^2\rho_i$ is the mass per unit length of the rope (assumed to be constant). The effective drag coefficient c_D is found to have value on the order of 1.

[8] Since a decrease of the ambient density and magnetic field and the flux rope expansion were not considered, the results do not reproduce all relevant aspects of the motion of CMEs. However, these simulations justify (at least in the absence of the magnetic reconnection) the application of the mentioned functional form for the drag (for a discussion, see *Cargill et al.* [1996]). This then provides analytical modeling of the IP motion of erupting flux ropes like, for example, those performed by *Chen* [1996].

[9] In paper 1 it was shown that the deceleration of the studied events can be expressed as $a_{\rm drag} = -\gamma_2|\upsilon - w|(\upsilon - w)$, where υ is the eruption speed and w is solar wind speed. Statistically, the coefficient γ_2 decreases with the heliocentric distance r at which the event was measured. The decrease can be approximately represented by the power law $\gamma_2 = \alpha_2 R^{-\beta_2}$, where $R = r/r_\odot$. In the considered radial distance range (say, $R < 15$) the average values of constants are found to be $\alpha_2 \approx 22\ 10^{-6}$ km^{-1} and $\beta_2 \approx 2.2$.

[10] Comparing with the previously mentioned expression for the drag acceleration, one finds $\gamma_2 = c_D\rho_e\lambda/m = (\rho_e/\rho_i)c_D/\pi\lambda$. This relation shows that γ_2 is directly affected by the CME radial expansion, i.e., by the increase of λ. On the other hand, the behavior of the ratio ρ_e/ρ_i depends on the ambient density decrease $\rho_e(r)$, the leakage of the cold prominence material [see, e.g., *Vršnak et al.*, 1993], and on the expansion of the CME volume. Let us note that in the IP space the density of magnetic clouds is not very much different from its surrounding [*Burlaga et al.*, 1987], whereas in the corona the ratio is, say, $\rho_e/\rho_i \approx 1/10$. So the increase of the ratio ρ_e/ρ_i is smaller than the increase of the flux rope radius λ, and thus γ decreases with the increasing r.

[11] Using $c_D \approx 1$ [*Cargill et al.*, 1996] and taking that at $R = 10$ the flux tube radius is of the order of $\lambda \approx 10^6$ km, one finds $\gamma_2 \approx 0.5$–$5\ 10^{-7}$ km^{-1} if CME is several times denser than the ambient corona. Similarly, taking that λ is of the order of 10^5 km at the height of 1 $r_\odot$, one finds $\gamma_2 \approx 10^{-6}$–10^{-5} km^{-1}. The obtained values are consistent with those obtained empirically in paper 1 (see Figure 5b therein).

[12] In the following we present a simple semi-empirical model for the motion of IP ejecta based on the assumption that in the IP space the dominant force is the aerodynamic drag and that the coefficient γ decreases with the heliocentric distance. The aim is to advance the prediction of the 1-AU transit times, which in the case of slow CMEs usually are shorter than predicted by the constant acceleration model proposed by *Gopalswamy et al.* [2000]. It will be demonstrated that the model proposed in the following also reproduces the in situ velocities measured at 1 AU much better than the constant acceleration model. Let us stress that in this paper we consider only the statistical aspect of the problem: The behavior of γ can be significantly different from one case to another because of different evolution of the flux rope radius λ and the ratio ρ_e/ρ_i which can hardly be inferred for individual events. However, in section 4 we propose the procedure that can be applied in the individual case studies, in particular, to the events in which the deceleration can be measured from coronographic observations.

2. Model

[13] The dynamics of an erupting magnetic flux rope is dominantly governed by the Lorentz force, the drag force, and the gravity [*Chen*, 1996]. The MHD models of *Chen* [1989, 1996] and *Vršnak* [1990] predict that the Lorentz force attains maximum below heights of several solar radii, consistent with the observations [*Vršnak*, 2001a]. At larger distances it becomes negligible. This happens primarily because of the increase of the dimensions of the electric current system. The self-inductance L of the system increases and, consequently, the total current I decreases to preserve the associated magnetic flux $\Phi = IL$ (for the discussion of a possible influence of the reconnection process, see *Vršnak* [1990]).

[14] Since the gravity can also be neglected (paper 1), the drag becomes a dominant force in the late phase dynamics of CMEs [*Chen*, 1996]. The equation of motion reduces to $\dot{\upsilon} = -a_{\rm drag}$. The acceleration caused by the drag can be expressed in an approximate form as $a_1^{\rm drag} = \gamma_1(\upsilon - w)$ [see, e.g., *Kleczek and Kuperus*, 1969, and references therein], where υ is the CME velocity and w is the solar wind speed. The empirical results presented in paper 1 and the numerical simulations by *Cargill et al.* [1995, 1996] show that the expression quadratic in velocity $a_2^{\rm drag} = \gamma_2(\upsilon - w)|\upsilon - w|$ might be more appropriate.

[15] As mentioned in section 1 the coefficient γ_2 (and, analogously, γ_1) is a function of r since the radius of the flux rope λ and the density ratio ρ_e/ρ_i change with the distance. These dependences can not be derived straightforwardly and expressed in a simple explicit form (see various approaches by *Vršnak* [1990], *Osherovich et al.* [1993], *Vandas et al.* [1995], and *Chen* [1996]). Therefore we will use the empirical expressions established in paper 1, relating in a statistical manner the average values of the parameters γ_1 and γ_2 with the heliocentric distance as $\gamma_{1,2} = \alpha_{1,2}R^{-\beta_{1,2}}$, where α and β are empirically determined constants.

[16] Neglecting the Lorentz force and the gravity in late phases of the flux rope eruption and choosing for the drag the expression linear in velocity, the kinematics is governed by the equation of motion:

$$\dot{\upsilon} = \alpha_1 R^{-\beta_1}(\upsilon - w), \tag{1}$$

where $\upsilon = \dot{r} = \dot{R}r_\odot$ denotes the radial velocity. Adopting for the drag the expression quadratic in velocity, the equation of motion becomes

$$\dot{\upsilon} = \alpha_2 R^{-\beta_2}(\upsilon - w)|\upsilon - w|. \tag{2}$$

Substituting $\dot{\upsilon} = \dot{R}dv/dR$ into (1) and (2) and using $\upsilon = \dot{R}r_s$, one finds

$$\frac{d\upsilon}{dR} = r_s\alpha_1 R^{-\beta_1}\left(1 - \frac{w}{\upsilon}\right) \tag{3}$$

and

$$\frac{d\upsilon}{dR} = r_s\alpha_2 R^{-\beta_2}\left(1 - \frac{w}{\upsilon}\right)|\upsilon - w|, \tag{4}$$

respectively.

[17] In the following it will be assumed that (1) or (2) can be applied also to the motion of IP ejecta. Then, applying some solar

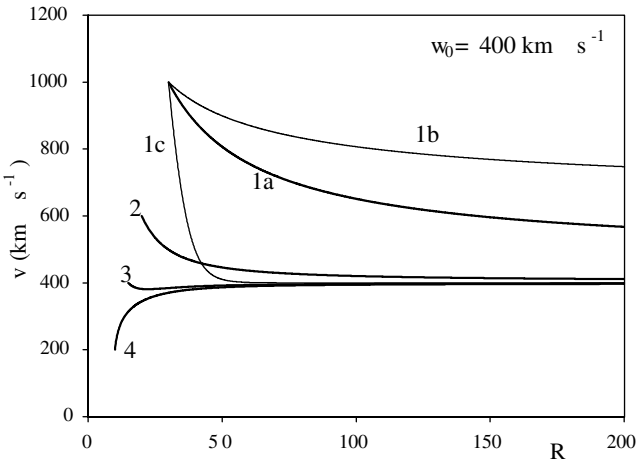

Figure 1. Motions $\upsilon(R)$ modeled using (3) and (5). The asymptotic solar wind speed was taken as $w_0 = 400$ km s^{-1}, and different distances of the driving force switch-off were assumed. Bold lines represent the deceleration with $\alpha_1 = 2 \times 10^{-3}$ s^{-1} and $\beta = 1.5$ for initial velocities of $\upsilon_0 = 1000$, 600, 400, and 200 km s^{-1} (curves labeled 1a, 2, 3, and 4, respectively). The curves labeled 1b and 1c represent the motion with $\alpha_1 = 10^{-3}$ s^{-1}, $\beta = 1.5$ and $\alpha_1 = 2 \times 10^{-3}$ s^{-1}, $\beta = 1$, respectively, using $\upsilon_0 = 1000$ km s^{-1}.

wind speed model, a numerical integration of (3) or (4) gives $\upsilon(R)$ and so $R(t)$.

[18] Bearing in mind the scatter of data points about the mean $\gamma(R)$ curves (see Figure 5 in paper 1) the integration was performed using a range of parameter values α and β. In Figure 1 the IP motion of CMEs is illustrated by showing the results of a numerical integration of (3) where different initial velocities $\upsilon_0 = \upsilon(t = 0)$ and several values of α_1 and β_1 are applied. The solar wind model by *Sheeley et al.* [1997],

$$w(R) = w_0 \sqrt{1 - e^{-\frac{R-2.8}{8.1}}}, \qquad (5)$$

was adopted. The asymptotic solar wind speed $w_0 = 298.3$ km s^{-1} proposed by *Sheeley et al.* [1997] was replaced in the calculations by $w_0 = 400$ km s^{-1} according to measurements of the 1-AU solar wind velocities [*Intriligator*, 1977]. Finally, it was assumed that the driving force is switched off at different heliocentric distances R_0 in the range $5 < R < 30$. It was found that the choice of the driving force switch-off distance R_0 plays a minor role in comparison with the choice of parameters α, β, and w_0.

[19] The results for $\upsilon_0 = 1000$ km s^{-1} are shown for different values of α_1 and β_1 to illustrate how the choice of these parameters affects the results. A similar outcome is found integrating (4) and using an appropriate choice of α_2 and β_2, e.g., $\alpha_2 = 5 \times 10^{-6}$ km^{-1} and $\beta_2 = 1.5$, or $\alpha_2 = 60 \times 10^{-6}$ km^{-1} and $\beta_2 = 2$. Figure 1 clearly shows a convergence of velocities toward the solar wind speed. The distribution of velocities of 23 CMEs and the associated IP ejecta presented by *Gopalswamy et al.* [2000] shows that the span of CMEs' velocities of 150–1050 km s^{-1} reduced at 1 AU to only 350–650 km s^{-1}. Bold curves in Figure 1 reproduce fairly well such behavior, indicating that $\alpha_1 = 2 \times 10^{-3}$ s^{-1}, $\beta = 1.5$, and $w_0 = 400$ km s^{-1} are a suitable set of parameters to reproduce the statistical behavior of the overall IP acceleration of ejecta.

3. Results

[20] Equations (3) and (4) were integrated numerically to determine the model transit times (T_{1AU}) and velocities (υ_{1AU}) of ejecta at 1 AU as a function of the initial velocity υ_0. The initial velocity range $\upsilon_0 = 200$–1500 km s^{-1} was considered. The solar wind velocity $w(R)$ described by (5) was applied, with w_0 ranging between 300 and 500 km s^{-1}. A set of values for α and β was used, bearing in mind the average coronal values obtained in paper 1. The heliocentric distance at which the deceleration begins was provisionally taken as $R_0 = 10$. The 1-AU transit time was then found as $T_{1AU} = T' + T'$, where T' is the travel time obtained integrating (3) or (4) and T' is the time needed to reach R_0 by the constant velocity υ_0. Let us stress that the results do not change much for any other reasonable choice of R_0, say, in the range 5–30 solar radii.

[21] The curves shown in Figure 2 are the model results $T_{1AU}(\upsilon_0)$ and $\upsilon_{1AU}(\upsilon_0)$ for several combinations of α, β, and w_0 which are chosen to illustrate a range of parameter values compatible with the observations. Solid circles show the observed arrival times of the leading edge of the ejecta from the list presented by *Gopalswamy et al.* [2000]. Crosses display the values $T_e = T + \tau$, where τ is the duration of a given IP ejection at 1 AU, i.e., T_e represents the 1-AU transit time for the trailing edge of an IP ejection.

[22] Analogous results obtained by integrating (4) are shown in the insets. Comparing these results with those obtained using (3), one finds that both models reproduce well the observed 1-AU transit times across the whole initial velocity range. However, Figure 2b indicates that the model based on (3) shows a better agreement with the observations when υ_{1AU} velocities are considered. Let us stress that among those shown, only the curves denoted by 1 in Figures 2a and 2b consistently reproduce the observed T_{1AU} and υ_{1AU}. For example, the curves labeled 3a and 3b in Figure 2a maybe better reproduce the observed arrival times T_{1AU} than curve 1, but the same set of parameters does not provide a good match with the observed values of υ_{1AU} (see curves 3a and 3b in Figure 2b).

[23] In Figure 3 some other models are compared with the observations. Beside the models governed by (3) and (4), the results obtained using $a = 0$ and $a = const$ [*Gopalswamy et al.*, 2000] are shown (curves labeled 3 and 4, respectively). Furthermore, the model considering a linear decrease of $a(R)$ is presented (a_{lin}; curve 5), adjusted to reproduce the average accelerations found by *Gopalswamy et al.* [2000].

[24] A discrepancy between the $a = 0$ model and the observations clearly shows that the drag acceleration is an essential feature of the IP motion of CMEs. The a = const and a_{lin} models are sufficiently accurate to predict the arrivals of fast CMEs, but slow CMEs with $\upsilon_0 \lesssim 300$ km s^{-1} arrive 1–2 days earlier than calculated. Furthermore, the dependence $\upsilon_{1AU}(\upsilon_0)$ is poorly matching the observations in the whole velocity range.

[25] The models based on (3) or (4) reproduce the observations better than the other models considered: The curves for $T_{1AU}(\upsilon_0)$ labeled 1 and 2 in Figure 3a lie by the slow events' data closer than the other three. Furthermore, the $\upsilon_{1AU}(\upsilon_0)$ dependence is much better reproduced (see Figure 3b), especially by the model based on (3).

4. Discussion and Conclusions

[26] In the proposed model it is taken into account that the main deceleration of fast IP ejecta occurs in the high corona. The transit times and velocities at 1 AU can be modeled reasonably well by using the simplest approximation for the drag acceleration $a_{drag} = -\gamma(\upsilon - w)$. Adopting the empirical model by *Sheeley et al.* [1997] for the solar wind velocity and using $\gamma = 2R^{-1.5}$, the model reproduces well the observations in the statistical sense.

[27] The calculated dependences $T_{1AU}(\upsilon_0)$ and $\upsilon_{1AU}(\upsilon_0)$ show that the 1-AU transit times and velocities in the events of a low initial speed depend on the solar wind speed more than those having a high initial speed. Inspecting the consistency of $T_{1AU}(\upsilon_0)$, $T_e(\upsilon_0)$, and $\upsilon_{1AU}(\upsilon_0)$ model curves with the observations, it can be

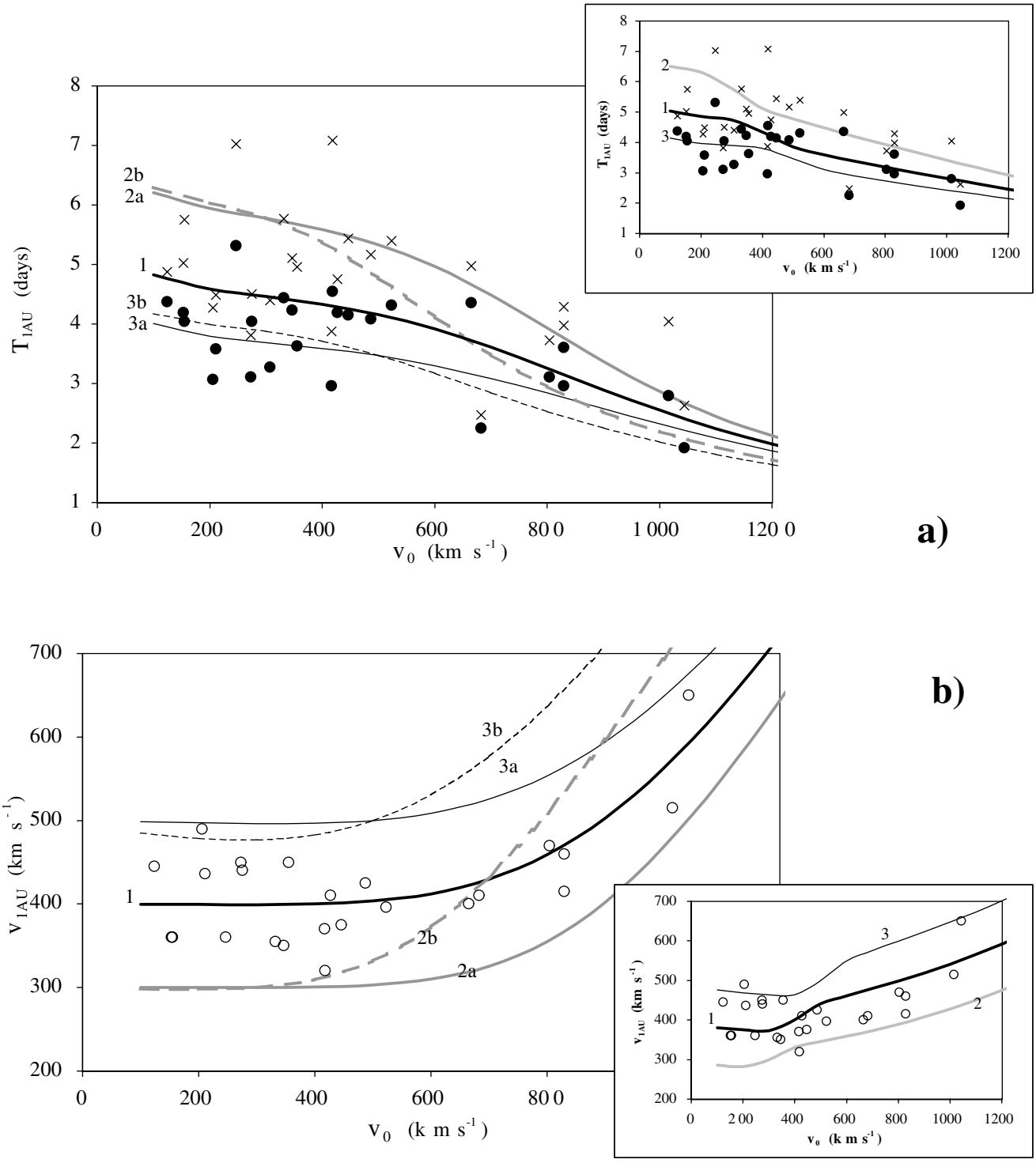

Figure 2. Comparison of the model results obtained using (3) with the observations. The results are shown for $\beta_1 = 1.5$. Bold, shaded, and thin solid lines (denoted as 1, 2a, and 3a) represent $\alpha_1 = 2 \times 10^{-3}$ s^{-1} with $w_0 = 400$ km s^{-1}, $w_0 = 300$ km s^{-1}, and $w_0 = 500$ km s^{-1}, respectively. Shaded and thin dashed lines (labeled 2b and 3b, respectively) are obtained using $\alpha_1 = 10^{-3}$ s^{-1} with $w_0 = 300$ km s^{-1} and $w_0 = 500$ km s^{-1}, respectively. The results based on (4) are shown in the insets for $\beta_2 = 2$ with $\alpha_2 = 60 \times 10^{-6}$ km^{-1}, where bold, shaded, and thin lines (labeled 1, 2, and 3, respectively) represent $w_0 = 400$ km s^{-1}, $w_0 = 300$ km s^{-1}, and $w_0 = 500$ km s^{-1}, respectively. (a) CME transit times T_{1AU} are shown versus the initial velocity υ_0. Closed circles and crosses represent the observed values $T_{1AU}(\upsilon_0)$ and $T_e(\upsilon_0)$, respectively. (b) The CME transit velocities υ_{1AU} are shown versus the initial velocity υ_0. Open circles represent the observed values $\upsilon_{1AU}(\upsilon_0)$.

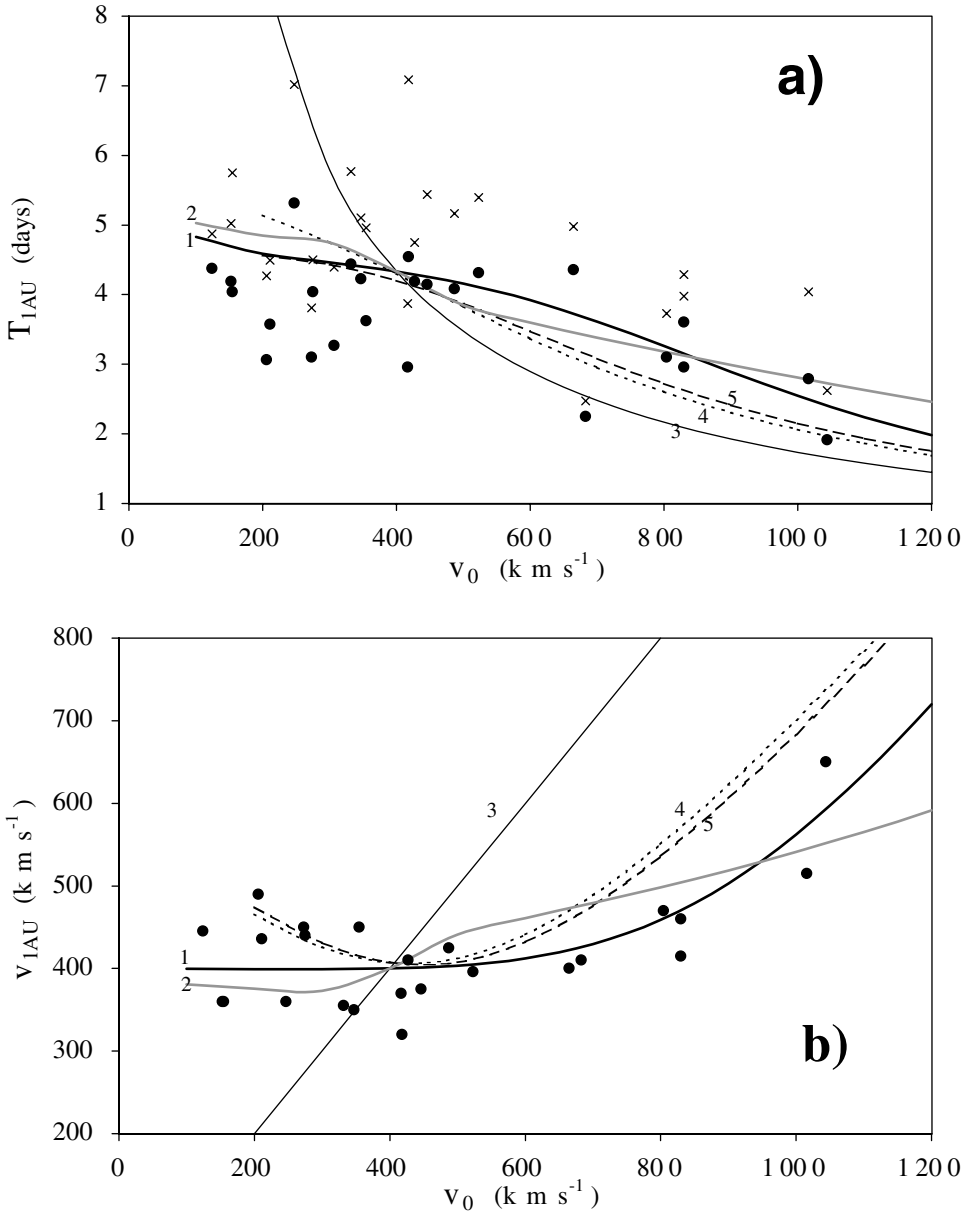

Figure 3. Comparison of different models with the observations. The model results are shown for $w_0 = 400$ km s^{-1}. The bold lines (labeled 1) represent the results obtained using (3) with $\alpha_1 = 2 \times 10^{-3}$ s^{-1} and $\beta_1 = 1.5$ (the same as the curves labeled 1 in the main graphs of Figure 2). The shaded lines (labeled 2) represent the results based on (4) for $\alpha_2 = 60 \times 10^{-6}$ km^{-1} $\beta_2 = 2$ (the same as the curves labeled 1 in the insets in Figure 2). The thin, dotted, and dashed lines (labeled 3, 4, and 5, respectively) represent the $a = 0$, a = const, and $a_{\rm lin}$ models, respectively. (a) CME transit times are shown versus the initial velocity υ_0. Circles and crosses represent the observed $T_{1AU}(\upsilon_0)$ and $T_c(\upsilon_0)$, respectively. (b) The 1-AU velocities υ_{1AU} are shown versus the initial velocity υ_0. Circles represent the observed values $\upsilon_{1AU}(\upsilon_0)$.

concluded that in the statistical sense the model results fit the best to a part of the IP ejecta that is somewhere between the leading and trailing edge, possibly associated with the location of the magnetic field maximum of the magnetic cloud [*Burlaga*, 1988].

[28] The solar wind transit times amount to $T_w = 5.8$, 4.3, and 3.5 days for $w_0 = 300$, 400, and 500 km s^{-1}, respectively. The group of low-velocity events ($\upsilon_0 \lesssim 400$ km s^{-1}) in Figure 2a, having transit times shorter than the solar wind of, say, $w_0 = 500$ km s^{-1}, can not be straightforwardly explained by the proposed model. A possible explanation is that the CME velocity was underestimated because of, for example, projection effects (Gopalswamy et al., submitted manuscript, 2001) or because they were still accelerating at the end of coronographic measurements. If so, the actual initial velocities υ_0 of these events were larger than considered, and the data points representing them in Figure 2a, in fact, should be shifted to the right, closer to the model curves. Another possibility is that in these events the solar wind speeds were close to 600 km s^{-1}, corresponding to $T_w = 2.9$ days.

[29] The solar wind speed is a highly variable parameter and on the spatial/time scale of an IP ejection it can vary as much as ±100 km s^{-1} (for the complexity of the problem, see *Burlaga et al.* [1987]). The wind speed measured at only one point (Earth), prior to the arrival of an ejection, might be thus taken only as a very crude estimate for the effective wind speed. Using such a value for the model input can introduce in some cases larger errors than using an average wind speed $w_0 \approx 400$ km s^{-1}.

[30] So, just the uncertainty in the values of the model input parameters υ_0 and w_0 introduces itself an error in estimating the 1-AU arrival time which can be up to ±1 day. The scatter of the observed values T_{1AU} at a given υ_0 (Figure 2a) is comparable with the estimated error, indicating that the mentioned effects probably represent a basic limitation in predicting the transit time of IP ejecta in general.

[31] A specific drawback of the proposed model is an uncertainty in the value of the parameter γ. The values used are based on an average scaling law. In individual case analyses, distinct values of the coefficients α and β should be assigned to each particular event: They depend on the initial value and the evolution of the flux rope radius λ and the density ratio ρ_e/ρ_i. This could be at least partly performed when an initial deceleration can be measured directly from the coronographic observations. Suppose that a CME is observed in the radial distance range between R_b and R_e, decelerating from the velocity υ_b to υ_e. In such a case the value $\gamma_0(\bar{R})$ can be estimated at $\bar{R} = (R_b + R_e) / 2$ from the deceleration rate $D([\bar{R}) = (\Delta\upsilon/\Delta r)_{\bar{R}}$, applying the procedure described in paper 1. Then the value of γ_0 can be used to adjust appropriately the value of α in (1) or (2). Furthermore, the solar wind velocity measurements in the considered period should be checked. If the speed prior to the arrival of the ejection was rather stable, it should be used as a hopefully good estimate for w_0.

[32] **Acknowledgments.** We are grateful to referees for very constructive comments and suggestions leading to a substantial improvement of the paper.

[33] Janet G. Luhmann thanks the referees for their assistance in evaluating this paper.

References

Burlaga, L. F., Magnetic clouds and force-free fields with constant alpha, *J. Geophys. Res.*, *93*, 7217–7224, 1988.

Burlaga, L. F., K. W. Behannon, and L. W. Klein, Compound streams, magnetic clouds, and major geomagnetic storms, *J. Geophys. Res.*, *92*, 5725–5734, 1987.

Cargill, P. J., J. Chen, D. S. Spicer, and S. T. Zalesak, Geometry of interplanetary clouds, *Geophys. Res. Lett.*, *22*, 647–650, 1995.

Cargill, P. J., J. Chen, D. S. Spicer, and S. T. Zalesak, Magnetohydrodynamic simulations of the motion of magnetic flux tubes through a magnetized plasma, *J. Geophys. Res.*, *101*, 4855–4870, 1996.

Chen, J., Effects of toroidal forces in current loops embedded in a background plasma, *Astrophys. J.*, *338*, 453–470, 1989.

Chen, J., Theory of prominence eruption and propagation: Interplanetary consequences, *J. Geophys. Res.*, *101*, 27,499–27,519, 1996.

Dryer, M., et al., Magnetohydrodynamic modelling of interplanetary disturbances between the sun and earth, *Astrophys. Space Sci.*, *105*, 187–208, 1984.

Gopalswamy, N., A. Lara, R. P. Lepping, M. L. Kaiser, D. Berdichevsky, and O. C. St. Cyr, Interplanetary acceleration of coronal mass ejections, *Geophys. Res. Lett.*, *27*, 145–148, 2000.

Gosling, J. T., and P. Riley, The acceleration of slow coronal mass ejections in the high speed solar wind, *Geophys. Res. Lett.*, *23*, 2867–2870, 1996.

Intriligator, D. S., The large scale and long term evolution of the solar wind speed distribution and high speed streams, in *Study of Travelling Interplanetary Phenomena 1977*, edited by M. A. Shea, D. F. Smart, and S. T. Wu, pp.195–225, D. Reidel, Norwell, Mass., 1977.

Kleczek, J., and M. Kuperus, Oscillatory phenomena in quiescent prominences, *Sol. Phys.*, *6*, 72–79, 1969.

Osherovich, V. A., C. J. Farrugia, and L. F. Burlaga, Dynamics of aging Magnetic clouds, *Adv. Space Res.*, *13*, 57–62, 1993.

Sheeley, N. R., Jr., et al., Measurements of flow speeds in the corona between 2 and 30 $R_\odot$, *Astrophys. J.*, *484*, 472–478, 1997.

St. Cyr, O. C., J. T. Burkepile, A. J. Hundhausen, and A. R. Lecinski, A comparison of ground-based and spacecraft observations of coronal mass ejections from 1980–1989, *J. Geophys. Res.*, *104*, 12,493–12,506, 1999.

Vandas, M., S. Fisher, M. Dryer, Z. Smith, and T. Detman, Simulation of magnetic cloud propagation in the inner heliosphere in two dimensions, 1, A loop perpendicular to the ecliptic plane, *J. Geophys. Res.*, *100*, 12,285–12,292, 1995.

Vandas, M., S. Fisher, M. Dryer, Z. Smith, and T. Detman, Simulation of magnetic cloud propagation in the inner heliosphere in two dimensions, 2, A loop parallel to the ecliptic plane and the role of helicity, *J. Geophys. Res.*, *101*, 2505–2510, 1996.

Vršnak, B., Eruptive instability of cylindrical prominences, *Sol. Phys.*, *129*, 295–312, 1990.

Vršnak, B., Magnetic structure of solar prominences, *Ann. Geophys.*, *10*, 344–353, 1992.

Vršnak, B., Dynamics of solar coronal eruptions, *J. Geophys. Res.*, *106*, 25,249–25,259, 2001a.

Vršnak, B., Deceleration of coronal mass ejections, *Sol. Phys.*, *202*, 173–189, 2001b.

Vršnak, B., V. Ruždjak, B. Rompolt, D. Roša, and P. Zlobec, *Sol. Phys.*, *146*, 147–162, 1993.

Watari, S., and T. Detman, In situ local shock speed and transit shock speed, *Ann. Geophys.*, *16*, 370–375, 1998.

Wu, S. T., R. S. Steinolfson, M. Dryer, and E. Tandbeg-Hanssen, Magnetohydrodynamic models of coronal transients in the meridional plane, IV, Effect of the solar wind, *Astrophys. J.*, *243*, 641–643, 1981.

B. Vršnak, Hvar Observatory, Faculty of Geodesy, Kačićeva 26, HR-10000 Zagreb, Croatia. (bvrsnak@geodet.geof.hr)

N. Gopalswamy, Department of Physics, Catholic University of America, Washington, DC 20064, USA. (gopalswamy@cua.edu)